THE JOURNAL OF BIOLOGICAL CHEMISTRY Vol. 278, No. 13, Issue of March 28, pp. 11513–11519, 2003

Printed in U.S.A.

High Resolution Structure of an Alternate Form of the Ferric Ion Binding Protein from *Haemophilus influenzae**

Received for publication, November 19, 2002, and in revised form, January 17, 2003
Published, JBC Papers in Press, January 17, 2003, DOI 10.1074/jbc.M211780200

Stephen R. Shouldice‡, Douglas R. Dougan§, Robert J. Skene§, Leslie W. Tari§, Duncan E. McRee§, Rong-hua Yu¶, and Anthony B. Schryvers¶‖

From the ‡Department of Biological Sciences, University of Calgary, Calgary, Alberta T2N 1N4, Canada, §Syrrx Inc., San Diego, California 92121, and the ¶Department of Microbiology and Infectious Diseases, University of Calgary, Calgary, Alberta T2N 4N1, Canada

The periplasmic iron binding protein of pathogenic Gram-negative bacteria performs an essential role in iron acquisition from transferrin and other iron sources. Structural analysis of this protein from *Haemophilus influenzae* identified four amino acids that ligand the bound iron: His^{9}, Glu^{57}, Tyr^{195}, and Tyr^{196}. A phosphate provides an additional ligand, and the presence of a water molecule is required to complete the octahedral geometry for stable iron binding. We report the 1.14-Å resolution crystal structure of the iron-loaded form of the *H. influenzae* periplasmic ferric ion binding protein (FbpA) mutant H9Q. This protein was produced in the periplasm of *Escherichia coli* and, after purification and conversion to the apo form, was iron-loaded. H9Q is able to bind ferric iron in an open conformation. A surprising finding in the present high resolution structure is the presence of EDTA located at the previously determined anion ternary binding site, where phosphate is located in the wild type holo and apo structures. EDTA contributes four of the six coordinating ligands for iron, with two Tyr residues, 195 and 196, completing the coordination. This is the first example of a metal binding protein with a bound metal·EDTA complex. The results suggest that FbpA may have the ability to bind and transport iron bound to biological chelators, in addition to bare ferric iron.

Iron plays a key role in many essential biological processes (1). Therefore, the acquisition of iron is integral for the survival of almost all organisms. Due to the low solubility of free ferric iron (Fe^{3+}) under physiological conditions, a variety of specialized systems for uptake, transport, and storage of this metal ion cofactor have been developed by living organisms (2). The majority of the iron obtained through the dietary intake in humans is stored and utilized in the intracellular compartment (3). Extracellular iron is complexed by the bi-lobed transport glycoprotein, transferrin (Tf),[1] within the body or by lactoferrin (Lf) on mucosal surfaces (4). These iron binding glycoproteins are produced in excess of free iron and bind iron at extremely high affinities ($K_d = 1 \times 10^{-21}$ M), effectively reducing the availability of this element, and thus protecting against bacterial infection (5, 6).

The ability of a pathogen to colonize and grow within the host is essential for the initiation of an infection (7). Thus to cause disease the pathogen must be successful in competing for protein bound iron in the host. In bacterial pathogens the expression of genes encoding iron acquisition proteins results from an adaptation to the iron-limiting environment within the host (8). Bacteria have diverse and elaborate systems capable of scavenging iron from host proteins. Some pathogenic microorganisms are able to synthesize and secrete low molecular mass (500–1000 Da) organic iron chelators termed siderophores, which are able to bind iron with association constants as high as 10^{53} (3, 9). This mechanism of iron acquisition is effective for a variety of different iron sources and environments and is typically found in bacteria that are present in a variety of different ecological niches. Iron is transported into the bacterial cell in the form of an iron chelate by this mechanism (9).

Another strategy is chelate-independent and employs an array of distinct outer membrane receptors, which specifically interact with the different host iron binding proteins. This mechanism is utilized by pathogenic bacteria of the Neisseriaceae (*e.g. Neisseria gonorrhoeae* and *Neisseria meningitidis*) and Pasteurellaceae (*e.g. Haemophilus influenzae*) families, which are not capable of producing siderophores (10, 11). These microorganisms produce Tf and Lf surface receptors that are capable of binding the iron-loaded host proteins as the first step in this elaborate iron acquisition system (12). The heterodimeric receptor complex typified by the Tf receptor is composed of two proteins, transferrin binding proteins A and B (TbpA and TbpB, respectively).

Even though the binding of iron-containing proteins to the bacterial surface receptors is well characterized, the subsequent steps of iron removal and transport into the bacterial cell are not well understood. The removal of iron from Tf and the subsequent transport of free iron across the outer membrane requires energy provided by TonB and its associated proteins, ExbB and ExbD (13). Once the iron is removed from Tf, and transported across the outer membrane, it is bound by the periplasmic ferric ion binding protein (FbpA) (14). The continued transport of Fe^{3+} from FbpA across the cytoplasmic mem-

* This work was supported by Grant 49603 from the Canadian Institutes for Health Research. The costs of publication of this article were defrayed in part by the payment of page charges. This article must therefore be hereby marked "*advertisement*" in accordance with 18 U.S.C. Section 1734 solely to indicate this fact.

The atomic coordinates and structure factors (code 1NNF) have been deposited in the Protein Data Bank, Research Collaboratory for Structural Bioinformatics, Rutgers University, New Brunswick, NJ (http://www.rcsb.org/).

‖ To whom correspondence should be addressed: Dept. of Microbiology and Infectious Diseases, University of Calgary, Rm. 274, Heritage Medical Research Bldg., 3330 Hospital Dr. NW, Calgary, Alberta T2N 1N4, Canada. Tel.: 403-220-3703; Fax: 403-270-2772; E-mail: schryver@ucalgary.ca.

[1] The abbreviations used are: Tf, transferrin; Lf, lactoferrin; FbpA and -B, ferric ion binding proteins A and B; TbpA and -B, transferrin binding proteins A and B; PLBP, periplasmic ligand binding protein; PEG, polyethylene glycol.

brane requires the genetically linked hydrophobic membrane protein, FbpB and the cytoplasmic membrane-associated nucleotide binding protein, FbpC, which together form a Fe^{3+} ATP-binding cassette transporter (15). Once inside the cytoplasm ferric iron is able to bind iron-coordinating proteins required for growth or be stored in the form of bacterioferritin (16).

A series of site-directed mutants of FbpA were prepared to evaluate the role of the various amino acid side chains in metal binding and their importance for the iron acquisition process. In this study, we report the 1.1-Å nominal resolution and 1.14-Å actual resolution (where the last shell is >50% complete) crystal structure of a holo *H. influenzae* site-directed mutant (H9Q) FbpA in complex with EDTA. With EDTA bound at the previously described anion-binding site, FbpA adopts an open conformation. Characteristics of the residues involved in EDTA binding show how FbpA may be able to accommodate a broad range of anion ligands. The EDTA molecule is able to fulfill the octahedral requirements of Fe^{3+} by contributing four of the required six ligands. This is the first example of a metal binding protein, which binds a metal·EDTA complex.

EXPERIMENTAL PROCEDURES

Purification and Crystallization Procedures—Escherichia coli BL21(DE3)/pLysS harboring the pT7-7 plasmid encoding FbpA with the His^9 to Gln mutation (H9Q) was used to express the *H. influenzae* mutant protein in the periplasm under isopropyl-1-thio-β-D-galactopyranoside induction. The protein was then purified using a modified osmotic shock procedure. Briefly, the broth culture was harvested by centrifugation at 4000 rpm for 20 min using a GSA rotor at 4 °C. The supernatant was discarded, and each pellet was resuspended in 1/10 volume (50 ml) of buffer composed of: 30 mM Tris/HCl buffer, pH 8.0, 20% sucrose, and 1 mM EDTA. The solution was rocked for 10 min at room temperature. The samples were then centrifuged at 4000 rpm for 30 min using a GSA rotor at 4 °C. The supernatant was again discarded, and the bottles were inverted onto paper towels briefly to remove all traces of supernatant. The pellets were rapidly resuspended in 10 ml of ice-cold 5 mM $MgSO_4$ by pipetting up and down with a 1-ml pipette. The solutions were left on ice for 20 min. After which time the samples were centrifuged at 4000 rpm for 30 min using a GSA rotor at 4 °C. The supernatant was carefully removed, without disrupting the pellet, because the supernatant contains the periplasmic osmotic shock fraction. Finally, the sample was extensively dialyzed against 10 mM Tris/HCl buffer, pH 8.0, at 4 °C.

Following dialysis, the protein sample was subjected to cation exchange chromatography on the Bio-Cad high-performance liquid chromatography system as a final purification step. The column was washed with 10 volumes of 20 mM Tris/HCl buffer, pH 7.5, to remove unbound proteins and eluted with a gradient of 0–1.5 M NaCl. The material collected from the column was concentrated to a final volume of between 1–3 ml using a Centricon 10 microconcentrator. The removal of iron from the protein was then accomplished by treatment of the protein in the Centricon 10 microconcentrator with 1 mM EDTA and a 4000-fold molar excess of citrate (sodium salt, pH 7.5) and incubation on ice for 20 min. At this point the protein, still in the Centricon, was exhaustively exchanged into 10 mM Tris/HCl buffer, pH 8.0. Once completed, 5 mM phosphate was added to the Centricon, and the sample was again incubated on ice for 20 min. After the incubation period, it was again washed extensively with 10 mM Tris/HCl buffer, pH 8.0. Finally, the sample was concentrated to ~25 mg/ml and iron was loaded. Iron-saturated FbpA was prepared by adding a 5-fold molar excess of a ferric citrate solution. A fresh ferric citrate solution was prepared by dissolving ferric chloride ($FeCl_3 \cdot 6H_2O$, Sigma) in 100 mM sodium citrate/100 mM sodium bicarbonate buffer. The protein and ferric citrate solution was then placed at 4 °C overnight before being used for crystallization or being frozen for later use. The resulting preparations were deemed pure based on SDS-PAGE analysis. All proteins were stored at −80 °C until they were used for crystallography.

The sitting-drop vapor diffusion method was employed for crystallization of the protein. All crystallization experiments were conducted at 20 °C with 4-μl drops containing Fe-FbpA, 10% (w/v) PEG 5000, and 50 mM Tris/HCl buffer solution at pH 8.2. The drops were equilibrated against a 1-ml reservoir containing 20% PEG 5000 and 100 mM Tris/HCl buffer, pH 8.2. Large, pink crystals of the protein grew within 1 week. These crystals were suitable for x-ray diffraction and belonged to the orthorhombic space group $P2_12_12$ (a = 105.1 Å, b = 75.3 Å, c = 33.6 Å).

Data Measurement—The crystals in a sitting drop were harvested by scooping them with a nylon loop. The crystal was then dipped into a cryoprotectant solution containing 30% (v/v) ethylene glycol, 100 mM Tris/HCl buffer, pH 8.2, and 20% (w/v) PEG 5000 for ~30 s before they were frozen in liquid nitrogen. Diffraction data were collected from a frozen crystal of the H9Q FbpA·EDTA·Fe complex up to 1.1 Å at 100 K using a QUANTUM4 charge-coupled device camera on Beamline 5.03 at the Advanced Light Source Berkeley Laboratory, Berkeley, CA, using a wavelength of 1.0 Å. The data were reduced and scaled using the HKL2000 software (17). The dataset statistics are given in Table I.

Structure Determination—The crystal structure was determined by a molecular replacement procedure using the program Molrep from the CCP4 suite of programs (18). The coordinates of the *H. influenzae* wild type apoFbpA (open conformation) were used as the search model. Iterative cycles of interactive manual refitting of the model using the program XtalView/xfit made use of maps created with ARP/wARP 5.2 and refinement with Refmac5 was carried out to complete and correct the model. During the later stages of refinement, difference maps ($F_o - F_c$ maps) were used to place the bound EDTA·iron complex. Restrained refinement using a maximum likelihood target function and anisotropic temperature factors for individual atoms was carried out. During the final refinement stage, well-defined residual electron density peaks in difference maps were assigned to water molecules. The last residue of the C terminus was not visible in the electron density map, so it was omitted. Several side chains of surface-exposed residues are also missing (residues 10, 11, 27, 43, 93, 119, 244, and 282) and were built as alanines. The final crystallographic R-factor is 0.158 for all data from 105.4- to 1.1-Å resolution. The free R-factor for randomly selected 5% data is 0.180.

Structure Analysis—The overall structure obtained for the mutant FbpA is similar to the previously reported metal-loaded and apoFbpA structures. The refined coordinates of *H. influenzae* H9Q FbpA in complex with EDTA·Fe have been deposited in the Protein Data Bank. Ramachandran plots of the mutant structure shows the satisfactory location of all residues into allowed regions of conformational space. The DALI server (www2.ebi.ac.uk/dali) was utilized to find structurally similar proteins in the Fold Classification Based on Structure-Structure Alignment of Proteins data base (19).

RESULTS

Crystal Production—The recombinant H9Q FbpA mutant protein was isolated from the periplasm of *E. coli* and purified by ion-exchange chromatography. Following conversion to the apo form, the protein was exhaustively exchanged into a 10 mM Tris/HCl buffer, pH 8.0. The production of an apo form allowed for the possibility of various metals to be added to the sample to determine binding affinities for the mutant protein (results not shown). A portion of the concentrated apo sample was iron-loaded with a 5-fold molar excess of ferric ions dissolved in a citrate/bicarbonate buffer for crystallization. Crystals grew within 1 week using the sitting drop method with 4-μl drops and a 1-ml reservoir of 20% PEG 5000 and 100 mM Tris/HCl buffer, pH 8.2, at 20 °C.

Structural Features—H9Q FbpA has the same overall topology as the apo form of wild type FbpA, with approximate dimensions of 60 Å × 30 Å × 40 Å (Fig. 1). The mutant protein, like the wild type FbpA is composed of two structural domains, termed the N and C domains. Each domain is composed of a twisted five-stranded mixed β-sheet surrounded by α-helices (Fig. 2). The two domains are connected by two antiparallel β-strands, which form the hinge between the two domains. Hinge bending between the two domains enables the participation of both domains in the binding and sequestering of the EDTA·Fe ligand.

Comparison of the H9Q FbpA crystal structure with that of the *H. influenzae* wild type FbpA structures reveals that the mutant protein is able to bind iron in an open conformation (Fig. 1). The Cα trace shows that the mutant protein form is highly similar to the apo wild type form. The root mean square deviation for 308 Cα atoms is only 0.50 Å, whereas the root

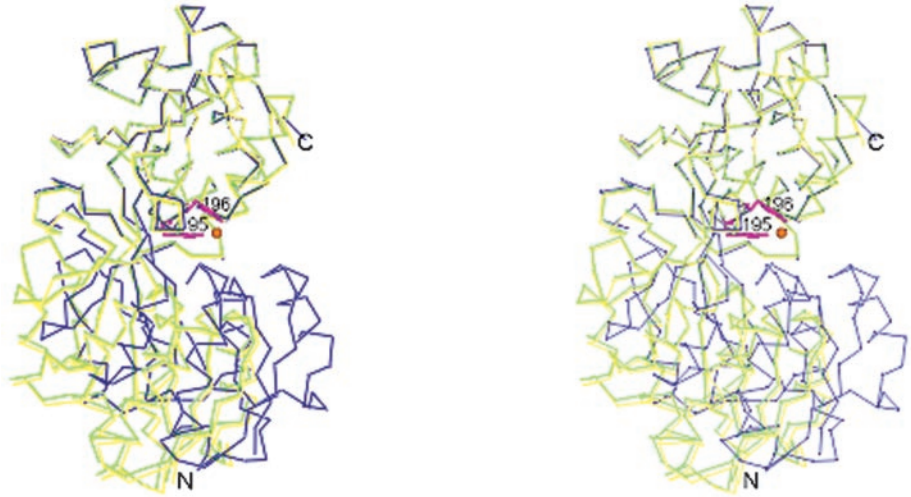

FIG. 1. **Stereo Cα plots of *H. influenzae* FbpA.** The apo (*yellow*) and holo (*blue*) forms of the wild type protein are superimposed with the H9Q structure (*green*). The figure was produced with XtalView/Xfit (34) and ViewerLite 5.0 (available at www.accelrys.com). The models are superimposed on the C domain. The holo and apo structures were derived from their respective pdb files (1MRP and 1D9V) from the Protein Data Bank. 1D9V was employed as the model for the current structural determination of the H9Q form. The iron-binding tyrosine residues (Tyr^{195} and Tyr^{196}) of the C domain are shown in *pink*, and the iron atom is in *orange*. The N-terminal domain is at the *bottom*.

FIG. 2. **Overall structure of H9Q FbpA complexed with EDTA·Fe.** A *stereo ribbon diagram* showing the overall tertiary structure and secondary structure elements in the complex. The EDTA molecule and iron atom are *black*. Helices, β-strands, and random coil regions are *gray*. This figure was produced using XtalView/Xfit (34) and ViewerLite 5.0. The N and C termini are labeled.

mean square deviation for the same 308 Cα atoms of the apo and holo structures is 5.55 and 5.76 Å when the mutant and wild type holo forms are compared.

The crystallographic refinement parameters (Table I) and the final electron density maps and Ramachandran plot (20) (not shown) of the main chain torsion angles as defined by the program PROCHECK (21) indicate that the crystal structure of H9Q is of high quality. In the Ramachandran plot 94.2% of the non-glycine residues are in the most favored regions and 5.8% are in additional allowed regions. This structure represents the first example of a metal binding protein with a bound metal·EDTA complex.

Iron and EDTA Binding Sites—Electron density maps showing the bound EDTA molecule and iron atom are displayed in Fig. 3. The high resolution electron density maps ($2F_o - F_c \alpha_c$ and $F_o - F_c \alpha_c$) resolving individual atoms allowed for the unambiguous placement of the EDTA molecule at the binding site. Other anions were considered based on buffers used during the purification and crystallization protocols, but they were later rejected due to their lack of agreement with the electron density maps.

A diagram of the EDTA·Fe binding site is displayed in Fig. 4. In this H9Q FbpA structure, the iron binding residues of the C-terminal domain (Tyr^{195} and Tyr^{196}) adopt essentially identical placements and conformations with respect to the iron atom as those in the wild type holoFbpA structure (22). However, the iron binding residues of the N-terminal domain (Gln^9 and Glu^{57}) adopt similar conformations to the wild type apoFbpA (23). These residues have rotated away from their iron binding locations and are hydrogen-bonded to residues

TABLE I
Summary of crystallographic data collection and refinement

Data collection	
Space group	$P2_12_12$
Cell dimensions	
a (Å)	105.10
b (Å)	75.34
c (Å)	33.50
Wavelength (Å)	1.0
Resolution (Å)	105.41–1.10
Completeness (%)[a]	86.2(36.1)
$I/\sigma(I)$	36.7(5.4)
R_{sym}[b]	0.044(0.199)
Redundancy	6.7
Refinement statistics	
Resolution (Å)	105.41–1.10
Completeness for range (%)	86.16
Number of reflections	89423
R-factor[c]	0.1582
R_{free}	0.1804
Number of protein atoms	4694
Number of water molecules	359
Ions	1 Fe/1 EDTA
Mean *B*-factor (Å^2)	9.042
Root mean square deviation from ideality	
Bond lengths (Å)	0.010
Bond angles (°)	1.257

[a] *Number* in *parentheses* is the statistic for the highest resolution shell.
[b] $R_{sym} = \Sigma|I - \langle I\rangle|/\Sigma|I|$.
[c] *R*-factor = $\Sigma_{hkl}\,|F_o - F_c|/\Sigma_{hkl}\,|F_o|$.

within their N-terminal domain across the groove from the iron atom. The distances of Glu^{57}-Oϵ1 and Gln^9-Oϵ1 from iron are 9.19 and 6.05 Å, respectively.

Filling the role of these two residues in the coordination of iron is a bound EDTA molecule. Because the EDTA is a rather large molecule, containing two nitrogen atoms and four carboxyl groups, it is also able to fulfill the roles of the phosphate anion and the water molecule that are found in the holoFbpA structure (22). The EDTA wraps around the iron atom, and one of the carboxyl groups is able to bind in the previously described ternary anion-binding site. As illustrated in Fig. 4, the EDTA provides four of the six coordinating ligands to iron binding. Thus, four oxygen donors and two nitrogen ligands still octahedrally coordinate the bound Fe^{3+}. The ligands include Tyr^{195}-OH, Tyr^{196}-OH, two EDTA oxygen atoms (O14 and O19), and the last two sites may be weakly coordinated by EDTA nitrogen atoms (N3 and N8) or almost empty, because the distances of these ligands from the iron are slightly longer (2.88 and 2.52 Å, respectively) when compared with the other

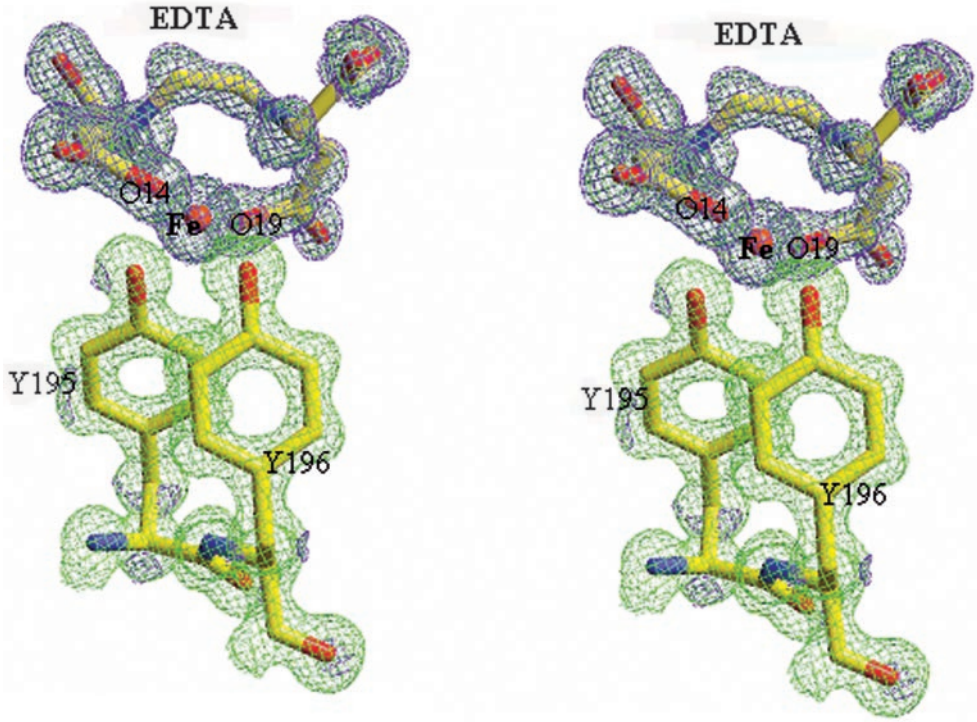

FIG. 3. **Stereo view showing the iron-binding site of the H9Q FbpA.** Electron density maps (*green*, $2F_o - F_c \alpha_c$ map, contoured at 1σ; *purple*, $F_o - F_c \alpha_c$ map, contoured at 2σ) were obtained using reflection data in which the EDTA and iron residues were omitted. This figure was made using XtalView/Xfit (34) and Raster3D (35).

coordination distances and distances previously reported for EDTA nitrogen atoms to Fe^{3+}. The iron coordination is distorted from perfect octahedral geometry, with distances ranging from 1.92 to 2.88 Å from iron to the coordinating ligands (Table II).

Previous small molecule crystallography on an EDTA·Fe complex revealed similar ligation geometry to that observed in the H9Q structure (24). The oxygen atoms in the small molecule structure that represent Tyr^{195}-OH and Tyr^{196}-OH in the H9Q structure have ligation distances of 1.98 and 2.10 Å, respectively. Also the oxygen atoms of EDTA in the small molecule structure that correspond to the coordinating EDTA oxygens (O14 and O19) in the H9Q FbpA have ligation distances of 2.10 and 1.97 Å, respectively. Although the above distances for oxygen atoms are very similar to those reported in Table II, the distances to the liganding nitrogen atoms in the H9Q structure are slightly longer than the previously reported distances of 2.32 and 2.32 Å for the same residues in the small molecule complex. The bond angles in the small molecule complex range from 71.8° to 106.0° (24). In H9Q the angles involving the nitrogen atoms deviate slightly from this range adding to the speculation that these residues may be coordinating the Fe^{3+} very weakly.

The EDTA molecule is well ordered with an average temperature factor of 17 $Å^2$. The binding of EDTA is stabilized by the location of one of the carboxyl groups in the previously determined anion-binding site. This carboxyl group is held in place by a similar constellation of residues as are shown to bind phosphate in the wild type apo and holo forms. The residues that contribute hydrogen bonds to this carboxyl group of EDTA include Asn^{175}, Asn^{193}, Ser^{139}, and Tyr^{195}. With a putative hydrogen bond also forming between the backbone nitrogen atom of Ala^{141} and the carboxyl group of EDTA. The other carboxyl group involved in the coordination of the iron interacts with the protein though hydrogen bonds with the side chain of Arg^{262}. These data suggest that there is a high degree of promiscuity in anion binding by FbpA and that FbpA is likely able to bind iron complexed with a wide range of chelators.

DISCUSSION

Analysis of the H9Q FbpA structure reveals that it adopts the typical periplasmic ligand binding protein (PLBP) fold that has been observed for almost all structurally determined PLBPs to date. Although PLBPs recognize a large variety of ligands and have very little sequence homology, almost all PLBP structures known to date are composed of two globular domains with the binding site located in a groove between these domains. The domains are connected by a number of flexible β-strands at the bottom of the ligand-binding site (25, 26). Even though FbpA possesses the typical PLBP structure, none of the other closely related periplasmic transport proteins bind naked metal atoms (27). A search using the DALI (19) server for proteins in the Protein Data Bank with similar three-dimensional folds to FbpA reveals structural similarity with sulfate binding protein, maltodextrin binding protein, spermidine binding protein, phosphate binding protein, and the N-terminal half-molecule of ovotransferrin.

Due to the striking structural similarity between transferrin and many periplasmic binding proteins, these proteins have been included in the transferrin structural superfamily (22). This group of proteins includes the eukaryotic transferrins, lactoferrins, and the bacterial periplasmic binding proteins, which transport a diverse group of ligands in the periplasmic space of bacteria. Despite operating in different organisms and cellular locations, human Tf and the *H. influenzae* FbpA appear to be structurally and functionally homologous (22). FbpA shares many structural similarities with each lobe of Tf, including two globular domains, each centered on a twisted mixed β-sheet surrounded by α-helices. In each protein a "hinge," which is composed of antiparallel β-strands, connects the two domains. Moreover, the coordination of the Fe^{3+} by the

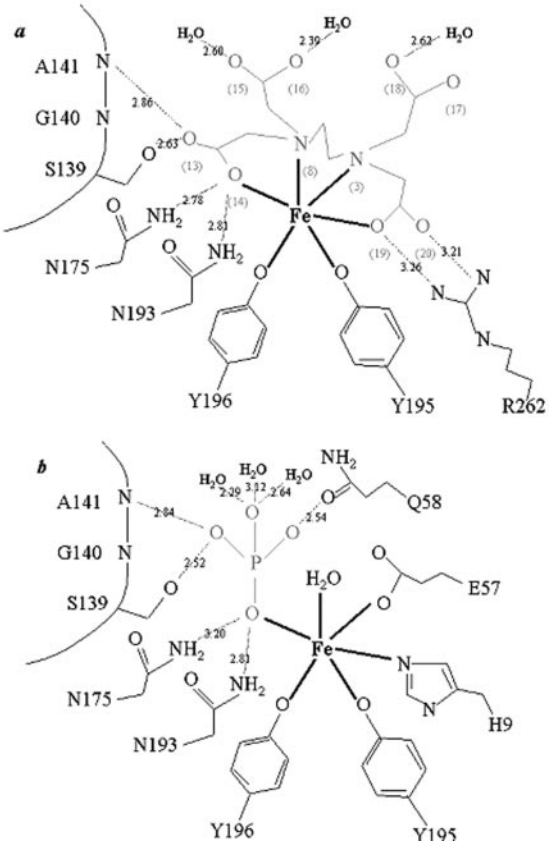

FIG. 4. **Diagram of the Fe^{3+} coordination and hydrogen bonding network.** *a*, the EDTA form; *b*, the holo form. The figure for the holo form is drawn using previous data (22) for comparison. The *thick solid lines* in *black* represent the possible coordination to Fe^{3+}, although the coordination by EDTA-N (3) and -N (8) are not clear because of longer iron to ligand distances than the other coordination distances (see Table II). The *dashed lines* in *black* display hydrogen bonds with the bond distances in angstroms. The synergistic anions (EDTA in *a* and phosphate in *b*) are shown in *gray*.

TABLE II
Geometry of the iron binding site

Bond lengths (Å)	
Fe-OH (Tyr^{195})	1.92
Fe-OH (Tyr^{196})	2.01
Fe-N3 (EDTA)	2.88
Fe-N8 (EDTA)	2.52
Fe-O19 (EDTA)	1.95
Fe-O14 (EDTA)	2.05
Bond angle (°)	
OH (Tyr^{195})-Fe-OH (Tyr^{196})	109.19
OH (Tyr^{195})-Fe-N3 (EDTA)	149.67
OH (Tyr^{195})-Fe-N8 (EDTA)	89.95
OH (Tyr^{195})-Fe-O19 (EDTA)	89.29
OH (Tyr^{195})-Fe-O14 (EDTA)	99.98
OH (Tyr^{196})-Fe-N3 (EDTA)	99.70
OH (Tyr^{196})-Fe-N8 (EDTA)	154.58
OH (Tyr^{196})-Fe-O19 (EDTA)	109.19
OH (Tyr^{196})-Fe-O14 (EDTA)	78.65
N3 (EDTA)-Fe-N8 (EDTA)	76.00
N3 (EDTA)-Fe-O19 (EDTA)	64.91
N3 (EDTA)-Fe-O14 (EDTA)	103.09
N8 (EDTA)-Fe-O19 (EDTA)	91.89
N8 (EDTA)-Fe-O14 (EDTA)	78.03
O19 (EDTA)-Fe-O14 (EDTA)	166.20

oxygens of two tyrosines, an imidazole nitrogen from histidine and a carboxylate oxygen from an acidic residue (Asp in Tf and Glu in FbpA), is identical (28). However, there are also some important structural differences between Tfs and FbpA. The first involves how each protein is able to complete the octahedral coordination of Fe^{3+}. Transferrin utilizes two oxygens from a carbonate anion, whereas FbpA makes use of an oxygen from a phosphate and another from a water molecule (22). Although the subset of amino acids coordinating the iron atom is very similar, the residues arise from different regions of the individual proteins. The iron-binding site is also more solvent-exposed in FbpA than it is in transferrin. The discrepancy in iron exposure is due to the binding site being shallower in FbpA and the absence of an additional loop covering the binding site in Tf.

Previous x-ray crystallographic analyses have illustrated that for those proteins of the transferrin structural superfamily for which both the apo and holo forms have been solved, the two domains rotate toward each other in the liganded structure (closed conformation) (8). The apo form of FbpA has the same overall topology as the holo form, however, the two domains of the protein are rotated about 20° with respect to each other (Fig. 1). A change in the dihedral angles of the antiparallel β-strands in the joining hinge region opens the binding site to the solvent.

Our initial intent was to determine the role of the metal-liganding residue His^9 in the coordination of iron in the *H. influenzae* FbpA. Site-directed mutagenesis was used to convert the histidine residue to a glutamine amino acid. In a companion study, the resulting mutant protein was tested for its metal-binding properties and ability to support transport of iron from transferrin.[2] As revealed by the present crystal structure the H9Q mutation has not affected the protein folding of FbpA (Fig. 1). However, the most interesting information gleaned from the H9Q structure is the protein's ability to bind iron in an open conformation with the use of an EDTA molecule. The presence of a bound EDTA molecule was very surprising given that EDTA was added only to convert the FbpA into an apo form and was not present in any subsequent solutions.

This high resolution structure provides valuable information for the structural pathway illustrating the conformational transition from the open to closed forms upon iron binding. The FbpA is fully iron-loaded, with the ordered iron-binding site of the C-domain occupied; yet the protein remains in an open conformation most likely due to the location of the EDTA molecule in the binding cleft. A similar structural state was reported for transferrin when crystallized with ferric nitrilotriacetic acid (29). Due to the fact that this FbpA·iron·EDTA complex formed in solution prior to crystallization, because EDTA and iron were absent from the crystallization conditions, two models can be proposed.

In the first model, EDTA binds in a mode that was first proposed for phosphate, based on the apo and holo structural information (22, 23). The EDTA molecule would likely be sequestered in the anion-binding site and close over the top of the iron once Fe^{3+} bound to the tyrosines. The other carboxylate group that is ultimately involved in iron coordination would likely have to remain free in this model until the Fe^{3+} is bound in order for the iron to have access to the tyrosines. This model is supported by the fact that during sample preparation the protein was washed extensively with buffer after which a large excess of phosphate was added to the sample, which was subsequently washed repeatedly with buffer again. The lack of phosphate in the present structure suggests that EDTA may have occupied the anion-binding site when phosphate was added to the solution and the favorable hydrogen bonds maintained the EDTA in position even during the buffer exchange protocol.

[2] A. G. Khan, S. R. Shouldice, R. Yu, and A. B. Schryvers, manuscript in preparation.

The second model assumes that the iron binds to the protein followed by the EDTA anion. In this model EDTA, either free in solution or associated with the protein at some other location, initially binds free ferric iron and then moves to the highly ordered iron-binding site involving the tyrosine residues (Tyr^{195} and Tyr^{196}) of the C domain or wraps over the top of the Fe^{3+} after the iron has bound to the tyrosine residues. Due to the steps involved during the sample preparation, the metal·EDTA complex would likely have to displace phosphate at the anion-binding site in this scenario. Regardless of the order involved, the present high resolution structure illustrates the point that ferric iron initially associates with the ordered tyrosine residues (Tyr^{195} and Tyr^{196}) of the C domain. The two domains would then rotate together as the histidine and glutamic acid residues are able to complete the coordination of free ferric iron in the wild type protein (22). The H9Q structure reveals how FbpA may be able to accommodate other metal·anion complexes.

A very important observation obtained from the H9Q structure with EDTA is the ability of a carboxyl group to occupy the anion-binding site. This was surprising, because the protein was also exposed to phosphate prior to the iron loading process. Previously it had been shown that a phosphate molecule was located at this ternary binding site (22, 23). The carboxyl group of EDTA found at the anion binding site forms hydrogen bonds with many of the same amino acids the phosphate anion was shown to bond to (Fig. 4). In the wild type holo form, PO_4^{3-} forms hydrogen bonds with Try^{195}-OH, Asn^{193}-Nδ2, Asn^{175}-Nδ2, Ser^{139}-Oγ, Ala^{141}-N, and Gln^{58}-Oϵ1. With the exception of Gln^{58}-Oϵ1, all of these moieties are hydrogen-bonded to the carboxylate group that occupies the anion-binding site. The other carboxylate group that is involved in the iron coordination is stabilized by hydrogen bonds to the protein residue Arg^{262}. The remaining two carboxylate groups of the EDTA molecule point out of the binding cleft and are hydrogen-bonded to water molecules. These groups of the EDTA molecule do not interact with protein residues in any way.

The observation of a carboxylate group occupying the anion-binding site rather than the previously determined phosphate is consistent with functional studies that demonstrated that a number of oxyanions can fill the role of the ternary anion (23, 30). Other groups have also discussed the ability of *H. influenzae* to grow in the presence of a number of iron chelates, with the present study providing an explanation as to how transport of these iron complexes may occur (31). This structure reveals how FbpA is able to not only bind free ferric iron but how it may be able to accept a variety of anions under physiological conditions.

It appears that the mutation of His^9 to Gln has very little effect on the present structure. The Gln residue adopts a very similar conformation to that of His in the apo wild type structure. The Gln residue rotates away from the iron binding site and hydrogen bonds with other residues present in the N-terminal domain. The glutamine is located across the cleft 6.05 Å away from the iron atom. Obviously, the Gln residue is unable to bind iron in the presence of EDTA due to steric hindrance. However, there seems to be no structural reason a Gln side chain could not coordinate to iron, as in theory it could coordinate iron through its amide oxygen. Primary sequence alignment of FbpA sequences from *H. influenzae* and *Pasteurella hemolytica* reveal that the histidine residue is replaced by a glutamine in the *P. hemolytica* protein. In fact, the crystal structure of the same histidine to glutamine mutation has been determined for the N-lobe of transferrin showing that this mutation is still able to octahedrally coordinate iron (32). However, it must be noted that the H249Q Tf structure may exist in the closed state, due to the increased number of interdomain interactions present in Tf that do not exist in the FbpA, because of to its more solvent-exposed cleft. Even though the H249Q transferrin protein is still able to coordinate iron in a closed conformation, spectroscopic studies have described altered properties, both in the acid stability of iron binding and the kinetics of iron release to chelators indicating a reduced affinity for iron (33). Thus, no conclusions can be reached at this point as to whether the H9Q FbpA would be a functional protein in the bacterium.

In conclusion, we have determined the first high resolution crystal structure of a metal binding protein, which binds a metal·EDTA complex. The previous crystallographic structures of FbpAs have been restricted essentially to the two structural forms: the first is the apo or open form, and the other is the holo or closed form (22, 23). As an alternate structural state, the current EDTA·Fe^{3+} structure is the first demonstration of an iron-loaded, open FbpA form. The high resolution structure allows for three important observations. First, only the two tyrosine residues (Tyr^{195} and Tyr^{196}) participate as protein ligands in the coordination of the iron atom. This observation provides evidence as to the entry of iron into the apo protein. Second, the presence of the carboxyl group stably bound in the anion-binding site instead of a phosphate anion, supports the idea of FbpA being able to use other available anions from the periplasmic space to coordinate iron. Finally, there is the observation of the ability of FbpA to bind a large molecule (EDTA) in the relatively shallow binding groove. The final observation proposes many more questions than answers. At this point in time we are unable to comment fully as to the significance of such a finding. Does this mean that wild type FbpA is able to accept and transport other iron complexes rather than just free ferric iron? Obviously, future studies on the H9Q and wild type proteins will have to explore this possibility. With such a shallow binding pocket compared with the transferrins, it is not unreasonable to speculate that FbpA may be able to bind biological iron chelate complexes, such as ferric citrate for transport into the bacterial cell. From the present study it is apparent that FbpA can accommodate much larger anions than phosphate.

Acknowledgment—We are indebted to Syrrx, Inc. for allowing the use of laboratory space and beam time toward the completion of this project.

REFERENCES

1. Weinberg, E. D., and Weinberg, G. A. (1995) *Curr. Opin. Infect. Dis.* **8,** 164–169
2. Braun, V., and Killmann, H. (1999) *Trends Biochem. Sci.* **24,** 104–109
3. Ratledge, C., and Dover, L. G. (2000) *Annu. Rev. Microbiol.* **54,** 881–941
4. Schryvers, A. B., and Stojiljkovic, I. (1999) *Mol. Microbiol.* **32,** 1117–1123
5. Griffiths, E., Chart, H., and Stevenson, P. (1988) in *Virulence Mechanisms of Bacterial Pathogens* (Roth, J. A., ed) pp. 121–135, ASM Press, Washington, D. C.
6. Crichton, R. R. (1990) *Adv. Protein Chem.* **40,** 281–363
7. Wooldridge, K. G., and Williams, P. H. (1993) *FEMS Microbiol. Rev.* **12,** 325–348
8. Clarke, T. C., Tari, L. W., and Vogel, H. J. (2001) *Curr. Top. Med. Chem.* **1,** 7–30
9. Neilands, J. B. (1995) *J. Biol. Chem.* **270,** 26723–26726
10. West, S. E. H., and Sparling, P. F. (1985) *Infect. Immun.* **47,** 388–394
11. Ogunnariwo, J. A., Cheng, C. Y., Ford, J. A., and Schryvers, A. B. (1990) *Microb. Pathog.* **9,** 397–406
12. Gray-Owen, S. D., and Schryvers, A. B. (1996) *Trends Microbiol.* **4,** 185–191
13. Stojiljkovic, I., and Srinivasan, N. (1997) *J. Bacteriol.* **179,** 805–812
14. Taboy, C. H., Vaughan, K. G., Mietzner, T. A., Aisen, P., and Crumbliss, A. L. (2001) *J. Biol. Chem.* **276,** 2719–2724
15. Sebastian, S., and Genco, C. A. (1999) *Infect. Immun.* **67,** 3141–3145
16. Andrews, S. C. (1998) *Adv. Microb. Physiol.* **40,** 281–351
17. Otwinowski, Z., and Minor, W. (1997) *Methods Enzymol.* **267,** 307–326
18. Collaborative Computational Project No. 4 (1994) *Acta Crystallogr. Sect. D Biol. Crystallogr.* **50,** 760–763
19. Holm, L., and Sander, C. (1997) *Nucleic Acids Res.* **25,** 231–234
20. Ramakrishnan, C., and Ramachandran, G. N. (1965) *Biophys. J.* **5,** 909–933
21. Laskowski, R. A., MacArthur, M. W., Moss, D. S., and Thorton, J. M. (1993) *J. Appl. Crystallogr.* **26,** 283–291
22. Bruns, C. M., Norwalk, A. J., Avrai, A. S., McTigue, M. A., Vaughan, K. A., Mietzner, T. A., and McRee, D. E. (1997) *Nat. Struct. Biol.* **4,** 919–924
23. Bruns, C. M., Anderson, D. S., Vaughan, K. G., Williams, P. A., Nowalk, A. J.,

McRee, D. E., and Mietzner, T. A. (2001) *Biochemistry* **40,** 15631–15637
24. Solans, X., and Font Altaba, M. (1984) *Acta Crystallogr. Sect. C Cryst. Struct. Commun.* **40,** 635–638
25. Quiocho, F. A. (1990) *Phil. Trans. R. Soc. Lond. Biol. Sci.* **326,** 341–351
26. Quiocho, F. A., and Ledvina, P. S. (1996) *Mol. Microbiol.* **20,** 17–25
27. Tam, R., and Saier, M. H. (1993) *Microbiol. Rev.* **57,** 320–346
28. Nowalk, A. J., Tencza, S. B., and Mietzner, T. A. (1994) *Biochemistry* **33,** 12769–12775
29. Mizutani, K., Yamashita, H., Kurokawa, H., Mikami, B., and Hirose, M. (1999) *J. Biol. Chem.* **274,** 10190–10194
30. Guo, M., Harvey, I., Yang, W., Coghill, L., Campopiano, D. J., Parkinson, J. A., MacGillivray, R. T. A., Harris, W. R., and Sadler, P. J. (2002) *J. Biol. Chem.* **278,** 2490–2502
31. Williams, P., Morton, D. J., Towner, K. J., Stevenson, P., and Griffiths, E. (1990) *J. Gen. Microbiol.* **136,** 2343–2350
32. Baker, H. M., Mason, A. B., He, Q. Y., MacGillivray, R. T., and Baker, E. N. (2001) *Biochemistry* **40,** 11670–11675
33. He, Q. Y., Mason, A. B., Pakdaman, R., Chasteen, N. D., Dixon, B. K., Tam, B. M., Nguyen, V., MacGillivray, R. T. A., and Woodworth, R. C. (2000) *Biochemistry* **39,** 1205–1210
34. McRee, D. E. (1999) *J. Struct. Biol.* **125,** 156–165
35. Merritt, E., and Bacon, D. (1997) *Methods Enzymol.* **277,** 505–524

High Resolution Structure of an Alternate Form of the Ferric Ion Binding Protein from *Haemophilus influenzae*

Stephen R. Shouldice, Douglas R. Dougan, Robert J. Skene, Leslie W. Tari, Duncan E. McRee, Rong-hua Yu and Anthony B. Schryvers

J. Biol. Chem. 2003, 278:11513-11519.
doi: 10.1074/jbc.M211780200 originally published online January 17, 2003
